J Inno Sci Eng, 2025, 9(2):295-308

DOI:https://doi.org/10.38088/jise.1721915

Research Article

Design of A High - Efficiency Inner-Rotor Permanent Magnet Brushless Direct Current Motor for General Applications

Halil Ercan KÖKSAL[1] Muhammed Fatih ÇORAPSIZ[2] *

[*]Department of Electrical & Electronics Engineering, Atatürk University, Erzurum, TR-25100, Türkiye

ARTICLE INFO

Received Date: 18/06/2025
Accepted Date: 14/07/2025

Cite this paper as:
Köksal H.E., Çorapsız, M. F. (2025). Design of A High - Efficiency Inner Rotor Permanent Magnet Brushless Direct Current Motor for General Applications *Journal of Innovative Science and Engineering.* 9(2), 295-308.

*Corresponding author: Muhammed Fatih ÇORAPSIZ
E-mail:corapsiz@atauni.edu.tr

Keywords:
BLDC Motor with Inner Rotor
Motor Design
Finite Element Method
2D Transient Analysis
High Efficiency Motor

ABSTRACT

In this study, it is aimed to design a Brushless Direct Current Motor (BLDC) with higher efficiency, speed and torque stability compared to asynchronous motors in applications such as fans, propellers, pumps, drills, lathes, ventilation, where asynchronous motors are generally used. The basic sizing parameters of the design were determined analytically, magnetic analysis and optimization of the dimension parameters were carried out through the ANSYS Maxwell program using the Finite Element Method (FEM). Since the designed BLDC is intended to be for general use and does not need additional cooling equipment, the output power is chosen as 1.5kW. The rated speed is determined as 1500 rpm in order to reduce switching losses. The design was tested by simulating different groove and pole numbers in the ANSYS Maxwell program and the highest efficiency was obtained with 9 grooves – 8 pole matches. Therefore, the motor is designed with 9 grooves and 8 poles.

1. Introduction

The Brushless Direct Current Motor (BLDC) first appeared in 1955 when Brailsford patented the first direct current motor without a Commutator. (Brailsford, 1955) **[1].** The structure used today was formed in 1962 when Wilson and Trickey developed the first Hall sensor BLDC **[2].**

BLDCs are used in many areas today due to their features such as being easy to manufacture, robust, having a high moment-to-volume ratio, showing high efficiency per unit volume, speed stability and ease of maintenance. **[3]**. For this reason, many studies have been conducted on the use of BLDC in different fields. In one of these studies, Yıldız conducted a study on the speed control of an BLDC's PI (proportional integral) controller and the Matlab simulation model for use in an underwater research robot. The design was carried out in the MATLAB Simulink program, and the torque and velocity changes of BLDC in both loaded and unloaded states were examined. It has been stated that with the increase in the amount of load on the motor shaft, the time for the motor to reach the reference speed is delayed, the motor works more stably at high speeds, and BLDC can be used in the underwater search robot **[4].**

Rahideh et al. designed an BLDC structure in the form of a non-grooved stator for use in medical devices. In this design, they used a genetic algorithm instead of FEM, which is commonly used in optimization processes. Using a genetic algorithm, they optimized the size, cost, and output power parameters of the engine. Demonstrating the effectiveness of the Genetic Algorithm in motor design, they stated that this method produced successful results in calculating the design parameters of high-efficiency motors **[5].**

BLDCs are also used in cooling and fan systems. However, the high cost of permanent magnets in the rotor increases the cost of BLDC production compared to the induction motor. Güney has made an BLDC design study with 12 grooves and 8 poles 250 W external rotor for use in smart cooling fan systems. A $250W$ induction motor has also been designed in order to compare the designed BLDC in terms of efficiency and cost. The sizing studies of both designs were carried out with the Ansys Maxwell RMxprt program and the magnetic analysis studies were carried out with the Maxwell 2D program. The designed BLDC and induction motor were compared in terms of efficiency and cost. As a result of the study, it was seen that it was more advantageous than the BLDC induction motor in terms of winding and production cost. However, it has been observed that the production cost is higher than the induction motor of BLDC due to the fact that the cost of magnets increases the total cost **[6].**

The stator structures of BLDCs are very similar to the stator structures of alternating current machines. Due to this similarity, there are also designs in which alternating current machines' stators are used as BLDC stators. Kandemir et al. manufactured an BLDC by placing position sensors on the stator of a $550W, 1.6A, 380V, 1390\ rpm$ 24-groove, 4-pole, star-connected asynchronous motor and permanent magnets of appropriate sizes on the rotor. They examined the change of phase current and phase voltage over time under $1\ Nm$ and $1.5\ Nm$ load conditions of the produced BLDC both in the simulation environment and in real time. The changes of phase current, phase voltage and output power obtained from simulation and experimental studies over time were compared. As a result of the study, it was shown that the structure obtained by using an asynchronous motor stator with a rotor of appropriate dimensions placed with permanent magnets can be used as BLDC **[7].**

BLDCs are widely used in electric vehicles today. In a study conducted for the development of BLDC designs that can be used in electric vehicles, Ocak designed a motor with a three-stage stator structure with a power of $1kW$, each with an external rotor. Dimension, magnetic analysis, simulation and optimization studies of the design were carried out with Ansys Maxwell RMxprt, Ansys Maxwell Simplorer and Maxwell 2D programs. The rotor magnets are placed on a single rotor pulley that wraps around all of the stators, with each group of rotors and stators working alone, two by two, or three together. It has been stated that the changes of the output power, input voltage and input current measured in real time after the motor production is carried out and the changes of the output power, input voltage and input current obtained as a result of the simulation made in ANSYS Maxwell are similar over time **[8].**

In another BLDC design study for electric vehicles, Aslan conducted a simulation study with BLDC's Ansys Maxwell program with an external rotor, $1.5\ kW$, 24 grooves and 20 poles for an electric vehicle with a weight of $90\ kg$ with its driver. Magnetic flux distribution, current density distribution, output moment – velocity, output power – velocity, input current – velocity, efficiency – velocity changes of the designed BLDC were examined. It was stated that the BLDC designed as a result of the study was suitable for the prototype electric vehicle **[9].** In one study, Virlan et al. proposed a 1.68 kW brushless direct current motor design with an in-wheel direct drive for electric vehicles with a 24-groove and 22-pole outer rotor. The design was carried out using the Ansys Maxwell RMxprt program and the magnetic two-dimensional analysis was performed through the Maxwell 2D software. It has been stated that the designed BLDC is an engine that can be used in electric vehicles **[10].**

When BLDC design is made for different usage areas, some engine design parameters need to be changed. Changing the value of any of the parameters selected for the design causes many features of the design characteristics to change. The values of the parameters used in the engine design are the values specific to that design. Motor designs with different numbers of grooves and poles for constant power also change the motor characteristics. Yetgin proposed an BLDC design with an inner rotor of 1.5 kW, $48V$ and 500 rpm with stator inner/outer diameter of $110mm$ and $210mm$, respectively, and rotor inner/outer diameter of 40mm and 108mm, respectively. In the simulation studies of the proposed BLDC, four different groove count values such as 18, 24, 30 and 36, were used and motor flux densities at pole numbers ranging from 8 to 34 were examined for each groove number. Stator and rotor yoke flux densities, magnet flux density, air gap flux density and stator female flux densities were analyzed with the Ansys Maxwell program for each number of grooves and each pole number. As a result of this study, it was stated that the design parameters and efficiency of the motor changed for each groove pole matching **[11].**

BLDC has the uniform velocity and torque characteristic of conventional direct current motors. BLDCs are more efficient than direct current motors because they do not contain brush-collector equipment, which is a disadvantage for traditional direct current motors . It has higher efficiency, less drive cost and a more stable speed-torque characteristic than BLDC induction motor **[12-14].**

Additionally, studies have been conducted examining the effects of different rotor structures on the output parameters of the BLDC. Çineli investigated the effect of the asymmetric rotor structure on the characteristics of the BLDC, such as cogging torque, back emf waveform, torque ripple, and motor efficiency. In this study, simulations were conducted using the ANSYS Maxwell program for three different designs: two BLDCs with different magnet thicknesses, one with a symmetrical and one with reduced magnet thickness, and one with a symmetrical structure but reduced magnet thickness. The study demonstrated that the asymmetric rotor structure was effective in reducing cogging torque, eliminating harmonic distortion in the back emf, and reducing torque ripple. It was observed that the torque constant increased with increasing magnet thickness in both symmetrical and asymmetrical rotor structures. **[15]**

In this study, it is aimed to make a general-use BLDC design that combines the superior aspects of asynchronous motors with the superior aspects of direct current motors, does not require additional cooling equipment, and has higher efficiency and speed sensitivity.

2. Material and Methods

BLDCs have structurally similar properties to other electric motors. Radial flux BLDCs are manufactured with an inner rotor and an outer rotor. In addition, BLDCs can also be manufactured with axial flux. In applications where low speed, constant speed or cogging moment is not desired, axial flux and low power BLDCs are used. In applications that require high torque and low speed or low inertia, BLDCs with internal rotors are preferred. In applications that require high speed and high inertia, BLDCs with external rotors are used **[3].**

In this study, it is aimed to design a general-purpose BLDC that can be used for general purposes with an internal rotor with $1500W$, $1500rpm$ and $220\,V$ inputs, which can be driven in a single phase by means of an BLDC driver with $1500W$ three-phase output, and which does not require additional cooling, in a completely closed form and more efficient than induction motors.

Analytical calculations in the sizing studies of the design were made through a program prepared in MATLAB. The calculated design parameters constitute the input parameters of the ANSYS Maxwell program. Using these parameters, sizing studies and magnetic analysis studies of the design were carried out. In general, the quantities that need to be determined/calculated for the design of an BLDC are presented below **[3]**.

1. Determination of application requirements

2. Deciding whether the motor will have an inner rotor, outer rotor or axial flux

3. Determination of magnet type

4. Determination of the number of poles

5. Determination of the number of grooves and phases

6. Rough sizing of the motor

7. Determination of air gap width and magnetic charge

8. Design of the rotor and determination of the amount of flux per pole

9. Determination of stator dimensions

10. Calculation of winding diameter, inductance and resistance per phase

11. Calculation of yield

12. Calculation of temperature rise, current and flux density

13. Evaluating the results and optimizing the design parameters until the desired level is reached.

2.1. Determination of Starting Motor Parameters for Motor Design

2.1.a. Determination of Application Requirements

In this study, an BLDC design with an internal rotor is planned for general use, does not need additional cooling equipment, can be supplied as a single phase and will not require a starting capacitor or auxiliary winding and centrifugal switch like single-phase induction motors, more efficient than induction motors, with a rated output power of $1500W\ and\ 1500\ rpm$ and an internal rotor.

2.1.b. Deciding Whether The Motor Will Have An Inner Rotor, Outer Rotor or Axial Flux

In this study, the BLDC design with an internal rotor was preferred. The reason why this design is preferred is that the internal rotor design has lower inertia, higher torque and the connection with the shaft can be made easier than the outer rotor type compared to the outer rotor design. In addition, since the engine planned to be designed is for general use, mechanical connections can be made much more easily.

2.1.c. Determination of Magnet Type

Ferrite, AlNiCo, SmCo, and NdFeB magnets are generally used as permanent magnets in BLDCs. Because the permanent magnet value of ferrite magnets is much lower than that of NdFeB magnets, the magnet size and motor size must be increased to achieve the desired magnetic flux density. Because this would increase motor size, weight, and efficiency, NdFeB 35 type magnets were used. NdFeB magnets have higher permanent magnet strength and physical strength than SmCo and AlNiCo magnets. As permanent magnets, rare earth magnets are widely used today in parallel with advances in technology. Among rare earth magnets, NdFeB N-35 type magnets are one of the most widely used magnets in BLDCs. Due to their high energy density, these magnets were preferred in the design. **[16]**

2.1.d. Determination of The Number of Poles

In motor design, the determination of the number of poles is directly related to the motor size and magnet size. In the BLDC design, the opposite emf waveform is in trapezoidal form, which is a characteristic feature of BLDC. In the BLDC design, it is seen that the opposite emf change occurs closer to the trapezoidal waveform as the groove number/pole number ratio approaches 1. For this reason, when determining the number of grooves and poles, the number of grooves/poles ratio is selected at values close to 1 and the windings are formed in the form of a condensed winding. The type of magnet and motor cooling used is directly effective in determining the size of the motor. For this reason, choosing a high number of poles and grooves for the determined motor size may cause a decrease in the groove and tooth width and magnetic saturation in the teeth. On the other hand, by selecting a low number of grooves and the number of poles, motor output torque and efficiency may decrease. First of all, a groove and pole number are selected as a start, and after the analysis, if necessary, the number of grooves and poles is changed and optimized. The mechanical frequency of a rotary machine at a speed of n rpm is f_m given by Equation (1).

$$f_m = \frac{n}{60} \tag{1}$$

$$f_e = \frac{np}{60} = pf_m \tag{2}$$

In equation (2), the expression of electrical frequency is f_e given. As seen in equation (2), the number of poles is inversely proportional to the number of revolutions. An increase in the number of poles at a constant electric frequency causes the number of revolutions to decrease. Choosing a high number of poles for a motor that is required to operate at a constant speed will increase the electrical frequency and cause the switching frequency to increase. Increasing the switching frequency increases switching losses, reducing motor efficiency and shortening drive life **[12,3].**

In this study, an 8-pole design was used for the calculated motor size and an N-35 type 5mm thick NdFeB magnet was used for the poles.

2.1.e. Determination of The Number of Grooves and Phases

The number of grooves and phases is directly related to the properties of the steel material used in stator lamellas, the number of poles, the size of the motor and the permanent magnetism value of the magnet. In this study, M350-50 type silicon alloy steel, which can give a flux density of 1.76 T without saturation at $10000 A/m$ magnetic field strength, was used **[17].** For this steel, a 9-groove design was chosen according to the size of the motor and with N-35 grade NdFeB magnets for 8 poles and 3 phases. While determining these values, simulations were made for different groove pole numbers with the ANSYS Maxwell program and the most appropriate values were tried to be obtained.

2.1.f. Motor Rough Sizing

In order to make the motor rough sizing, the basic motor output power, mechanical angular velocity (ω_m), electrical angular velocity and number of revolutions (n), as well as power (P),, torque (τ), mechanical angular velocity (ω_m), electrical angular velocity (ω_e), are given in Equation (3), Equation (4) and Equation (5), respectively.

$$P = \tau \,.\, \omega_m \tag{3}$$

$$\omega_m = \frac{2\pi n}{60} \tag{4}$$

$$\omega_e = p\omega_m \tag{5}$$

The nominal torque value required for the output power and number of revolutions determined by equation (3) is calculated. Then, according to the intended use of the motor, the ratio of the rotor radius to the rotor length (λ_{rl}) and the ratio of the rotor radius to the stator radius (λ_r) are determined. After determining these ratios, it is applied to Equation (6) for the torque value calculated by empirically determining the torque value per unit rotor volume (Torque Per Rotor Volume = TRV) obtained in previous studies and applications according to the magnet, lamination steel and motor cooling type and included in the literature, and the rotor volume (V_r) is found **[13].**

$$V_r = \frac{\tau}{TRV} \tag{6}$$

$$L_r = \frac{r_{ro}}{\lambda_{rl}} \tag{7}$$

$$r_{ro} = \sqrt[3]{\frac{V_r\, \lambda_{rl}}{\pi}} \tag{8}$$

$$r_{so} = \frac{r_{ro}}{\lambda_r} \tag{9}$$

In these equations, V_r is the rotor volume, τ output torque, TRV amount of torque per unit rotor volume, L_r rotor length, r_{ro} rotor outer radius, λ_r ratio of rotor radius to stator radius, λ_{rl} ratio of rotor radius to rotor length, r_{so} stator outer radius. In fully enclosed and naturally air-cooled engines, its value varies between $20\ kN/m^3$ and $42\ kN/m^3$. In this study, M350-50 type silicon alloy steel with average properties was used. The B-H curve for this steel is shown in Figure (1).

Figure 1:M350-50 Type Steel B-H Curve **[19]**

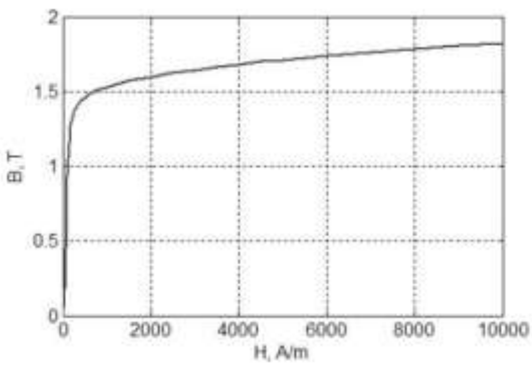

Figure 1:M350-50 Type Silicon Alloy Steel B-H Curve.[21]

The λ_r and λ_{rl} ratios are specific to the design and are determined by the designer based on the intended use of the design. The slot cross-section and stator tooth cross-section will be formed according to the stator radius determined by these ratios. Therefore, the slot cross-section must provide sufficient space for the wire cross-section to be used in the stator windings. Furthermore, the stator tooth cross-section must be wide enough to carry the magnetic flux density generated in the stator tooth cross-section without magnetic saturation. In this design, an optimum rotor radius/stator radius ratio of 0.5 was adopted to ensure that the winding provided would provide the required cross-section, based on the TRV value and rated power, and that the stator tooth cross-section could also carry the resulting magnetic flux density.

The properties of M350-50 type steel from three different manufacturers are shown in Table (1).

Manufacturer	**Minimum Magnetic Polarization Value (T)**		
	2500 A/m	**5000 A/m**	**10000 A/m**
Isovac	1.58	1.66	1.78
Thyessenkrupp	1.50	1.60	1.70
SIJ Acroni	1.50	1.60	1.70

Tablo 1: Minimum Polarization Values for M350-Type Steel at Magnetic Field Intensities of 2500 A/m, 5000 A/m and 10000 A/m from 3 Different Manufacturers **[18-20]**

When more than one manufacturer's catalogue is examined for M350-50 type steel, it can be seen that its magnetic properties are at average values. Therefore, the TRV value was taken as 30 on average. Selecting a high TRV value results in a higher torque value per unit rotor volume. This, in turn, will create a need for more magnetic flux density.

However, the design made according to the steel material used and the rotor and stator volumes calculated according to the TRV value may not provide some desirable features. Due to the low volume of the calculated groove, the current carrying capacities of the conductors to be placed may not be sufficient for the planned design. In addition, the low stator tooth cross-sectional area may cause the magnetic flux density to bring the core to magnetic saturation. Therefore, when selecting the TRV value, the flux density of the magnet used and the winding filling rate in the stator windings should be taken into account.

While the winding filling rate is between 35% and 45% in double-layer full mold windings, this rate can be between 60% and 75% in single-layer mold winding or hand wrapping **[14,16].** Equation (7) determines the rotor radii, and Equation (8) determines the stator radii. Equation (9) finds the rotor and stator lengths. In this study, and was taken as and $\lambda_r = 1/2\ \lambda_{rl} = 1/2$ the rotor radius was calculated as 40 mm, the stator radius was 80 mm, and the rotor and stator lengths were 80 mm.

EMF constant method, BLV method and Tooth Flow Method are used to determine the number of turns **[13].** The BLV method was used in this study. The magnitude of the opposite emf to be induced in the windings is given by Equation (10), where B_g is the flux density of the air gap, m is the number of phases, N is the total number of turns in a phase, ω_m is the mechanical angular velocity, L_{st} is the stator length (motor axial length),r_{si} the inner radius of the stator **[21].**

$$e = 2pB_gNL_{st}r_{si}\omega_m \quad (10)$$

Equation (10) can be used to find the number of turns. The total number of windings per phase at this number of revolutions is given by Equation (11) by equalizing the induced emf for the rated number of revolutions to the source voltage **[21].**

$$N = \frac{e}{2pB_gL_{st}r_{si}\omega_m} \quad (11)$$

The value of N found by equation (11) is the value of the number of turns per phase. To determine the number of turns in a groove of a phase, the total number of windings is divided by the number of coils per phase. The number of coils per phase varies according to the type of winding used and the number of layers. In this study, full mold winding was used. In full die winding, the total number of coils is equal to the number of stator grooves. C, the number of coils per phase; S, the number of grooves; where m is the number of phases; The number of coils per phase is calculated by Equation (12) **[21,13,22].**

$$C = \frac{S}{m} \quad (12)$$

In this case, the number of turns per phase in a groove is determined by Equation (13).

$$N_s = \frac{N}{C} \quad (13)$$

For the calculation of the input current, the Biort-Savart Law is applied. If the force acting on the wire on the armature is multiplied by the inner radius of the stator F, the value of torque induced in the motor for a coil edge is found. A coil consists of two coil edges. Therefore, the torque value found for a coil edge is multiplied by two to find the torque value induced in a winding. If this value is multiplied by the number of turns per phase, the torque value per phase is found. In the BLDC study, since only two phases are energized in each case, the torque induced in the motor will be equal to the torque value induced in two phases. $F = BIL\ Sin\ (\theta)$. In this case, the torque value produced in the BLDC rotor is given by Equation (14) **[21, 14].**

$$\tau = 4B_g INL_{st}r_{si} \tag{14}$$

Using equation (14), the input current I can be calculated. For this, Equation (14) is changed and written as in Equation (15). If the torque value calculated by Equation (3) is substituted in Equation (15), the current value I is obtained.

$$I = \frac{\tau}{4B_g NL_{st}r_{si}} \tag{15}$$

In this study, 9 grooves, 8 poles, 3 phases, 1 coil step Double Layer Lap Winding was used. In this case, there will be a total of 9 coils in the motor stator, and there will be 3 coils per phase.

In equation (15), $B_g, I, N, L_{st}, L_r, r_{si}$ shows the air gap flux density, line current, total number of turns in a phase, stator and rotor length, stator inner radius, respectively. In this study, the rotor length and the stator lamella package length were taken equally. With equation (15), the input current was calculated approximately and the conductor cross-section was selected according to the current density value. 6.85 $AJ = 5\ A/mm^2$ **[13].**

2.1.g. Determination of Air Gap Width and Magnetic Charge

For medium and large size motors, it is generally accepted that the air gap is 0.5mm or 1mm **[12].** In this study, it was selected as 1 mm for reasons such as ease of manufacturing, magnet thickness and efficiency.

In order to determine the air gap flux density, it is necessary to know the internal reluctance of the magnet, the air gap reluctance and the permeability coefficient of the magnet for the accepted temperature of $75\,°C$, the leakage coefficient, the reluctance coefficient and the permanent magnetism value of the magnet used. For this, the required quantities can be calculated using Equations (16), (17), (18) and (19), namely t_m magnet thickness, g air gap thickness, A_m magnet surface area, A_g air gap area, μ_r relative magnetic permeability of the magnet, μ_0 magnetic permeability of the cavity, P_C magnetic permeability constant, K_l leakage coefficient, K_r reluctance coefficient, R_m magnet reluctance, R_g air gap reluctance and B_g air gap flux density **[12].**

$$R_m \frac{t_m}{\mu_r \mu_0 A_m} \tag{16}$$

$$R_g \frac{g}{\mu_0 A_g} \tag{17}$$

$$P_C \frac{t_m A_g}{g A_m} \tag{18}$$

$$B_g = \frac{K_l C_\phi B_r}{1+K_r \frac{\mu_r}{P_C}} \tag{19}$$

In equation (18), ~~it~~ K_r takes values in the range $1 \leq K_r \leq 1.2$, K_l in the range of $0.9 \leq K_l \leq 1$ and takes its value for N35 grade magnets $\mu_r = 1.05$. (Hanselman, 2009). The magnetic flux density in the air gap is calculated to be approximately 0.9 T.

2.1.h. Design of The Rotor and Determination of The Amount of Flux Per Pole

In this design, the rotor is designed with surface magnets in order to increase efficiency and provide ease of production. The width of the magnet is taken as 0.9 of the width of the pole. In NdFeB magnets, the residual magnetism value is $B_r = 1.2\ T(W/m^2)$. In surface magnet motors, the ratio of air gap flux to magnet flux varies between 0.85 and 0.95 **[13].**

2.1.i. Determination of Stator Dimensions

When determining stator dimensions, the proportions λ_r and λ_{rl} are determined by the designer . These ratios are then substituted in Equation (7), Equation (8) and Equation (9) to find the stator radius and motor length. In this study, the rotor length for the preferred ratios was found to be 80 mm. The rotor length is taken to be equal to the stator length. The stator radius was found to be 80 mm.

Different numbers of grooves/poles can be applied in stator design, but it is important that the tooth width and air gap flux density to be formed according to these groove and pole numbers ~~are~~ at a level that will not cause saturation in the teeth. Many steel materials reach saturation after a magnetic flux density of 1.8 T and 1.9 T. For this reason, it is often desirable in motor design that the flux density in the stator teeth does not exceed 1.6 T **[3].** In selecting the slot geometry, the slot type with linear sections and shown as slot Type 3 in the Ansys Maxwell program was chosen in order to calculate the slot area, stator tooth cross-section exactly and, accordingly, the slot occupancy rate and winding wire cross-section calculation clearly. Stator groove and thread design are often processes that need to be optimized by trying different combinations. In this study, these procedures were performed using the ANSYS Maxwell program.

2.1.j. Calculation of The Diameter of The Winding

Double-layer Lap Winding is widely used in BLDCs for higher moment. In this type of winding, there are as many bobbins as the number of grooves in the machine.

After determining the number of turns, it is necessary to determine the winding wire cross-section for the closed and air-cooled motor type. The winding wire diameter depends on the rated current of the motor, the current density in the windings, the operating temperature, the type of cooling of the motor, and the structure of the winding. The engine designed in this study is planned to be a closed-form engine that does not need additional cooling equipment. According to this type of cooling, the upper limit of the current density is 5 A/mm^2 **[13].**

D_w The bare conductor diameter of the winding wire is given by Equation (20) for air-cooled motors, where the bare conductor diameter of the winding wire is the input current I.

$$D_w = \sqrt{\frac{I}{5\pi}} \tag{20}$$

2.2. Motor Efficiency Classification

Engine efficiency classes vary according to standards that differ according to countries or regions. CEMEP and IE in the European region and NEMA in the USA are the main organizations that set these standards. CEMEP is outdated and the current standards used in the European Union are IE standards. In our country, standards based on IE standards are determined by TSE. TS EN 60034-30-1 standard is still in force. This efficiency standard is also regulated according to the IECC 60034-2-1 standard **[23,24].** According to the IECC 60034-2-1 standard, the motor efficiency table is given in Table (2).

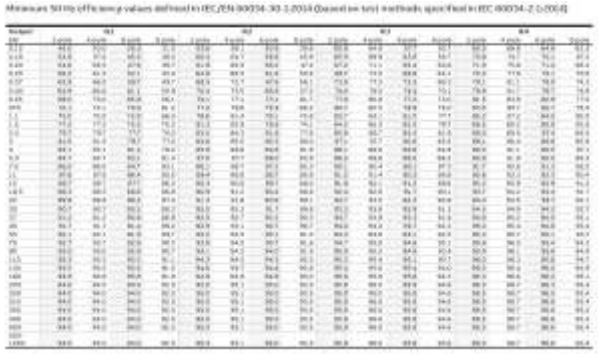

Table 2: IECC 60034-2-1-2014 Standard Motor Efficiency Classification by Motor Power and Number of Poles **[25]**

In this study, the parameters required to be entered into the Ansys Maxwell Program for BLDC design were analytically calculated. Rotor outer radius (r_{ro}), stator outer radius (r_{so}), stator tooth width (w_t), stator yoke width (w_{sb}), stator winding wire diameter (D_w) and number of turns per phase (N) values were calculated analytically with the MATLAB program. The parameter values calculated with this program were entered into the ANSYS Maxwell program and FEM analysis was performed. The input parameters calculated for FEM analysis of the designed $1500\ W, 1500 rpm, 220\ V$, 9 Groove, 8-pole BLDC are given in Table (3).

Table 3:Design Parameters for 1500 W 1500 rpm 220 V BLDC FEM Analysis

Design Parameter	Symbol	Value
Engine Power	P	1500 $Watts$
Number of	n	1500 rpm
Voltage	V	220 $Volts$
Number of Grooves	S	9
Number of Poles	$2p$	8
Number of Phases	m	3
Torque Value Per Unit Rotor Volume	TRV	30 kN/m^3
Stator Outer Radius	r_{so}	80 mm
Stator Inner Radius	r_{si}	41 mm
Rotor Outer Radius	r_{ro}	40 mm
Rotor Inner Radius	r_{ri}	10 mm
Package Length	L_{st}	80 mm
Number of Windings Per Phase	N	102 Tur
Stator Tooth Width	w_t	22 mm
Stator Yoke Width	w_{sb}	6.62 mm
Stator Lug Width	w_{sh}	24.62 mm
Default Air Gap Width	g	1 mm
Magnet Thickness	t_m	5 mm
Permanent Magnet Permanent Flux Density	B_r	1.2 T
Air-Gap Flux Density	B_g	0.9 T
Stator-Teeth Flux Density	B_t	1.22 T
Rotor Radius/Stator Radius Ratio	λ_r	0.5
Rotor Radius/ Rotor Length Ratio	λ_{rl}	0.5
Stator Lug Height	h_{s0}	3 mm
Stator Lug Neck Height	h_{s1}	2 mm
Gutter Height	h_{s2}	22 mm
Gap Between Lugs	b_{s0}	4 mm
Gutter Ceiling Width	b_{s1}	10
Gutter Base Width	b_{s2}	26

2.3. Cogging Torque

In BLDCs, the rotor permanent magnets and stator teeth are aligned at a position where the air-gap reluctance is minimum. Changing this position causes the air-gap reluctance in the path of the magnet magnetic flux to increase. Due to the increased reluctance in the path of the magnet's magnetic flux, the magnetic flux tends to complete the flux path at the position where the magnetic reluctance is minimum. This causes the magnetic flux to generate a moment in the direction opposite to the moment forcing the position change. This resulting moment is called cogging torque. Cogging torque is an undesirable effect in BLDCs because it creates torque fluctuations and vibration. Various methods are available to reduce cogging torque. Examples of these methods include skewed placement of rotor magnets, inclined design of stator teeth, and fractional winding. In this study, fractional winding was used in the design and the maximum value of the cogging torque was calculated as 192.935 mNm as a result of FEM analysis using the ANSYS Maxwell program. **[12, 3, 13]**

2.4. Finite Element Method (FEM)

The finite element method is a method that goes from the part to the whole. The finite element, on the other hand, is a part of the structure to be examined. The first area of application is stress analysis. Later, it was also applied to the fields of thermal analysis, magnetic analysis, and electrical analysis. Due to the fact that the problems encountered in engineering fields cannot be fully expressed analytically, the analyzed object or environment geometries are divided into smaller parts and a network structure is created with these elements. This structure is called a numerical model. The points where the elements that make up the numerical model come into contact with each other are called nodes. Each node has x, y, and z coordinates relative to a specific starting point. The main purpose of the finite element method is to represent continuous functions with regional continuous functions. In the finite element method, the value of the magnitude to be calculated in an element is found by interpolation using the values of that element at the nodes. The fact that the number of elements is as high as possible allows the feature to be determined to be calculated with a higher precision. A representation of the element and network structure used in FEM analysis is shown in Figure (2) **[26, 27].**

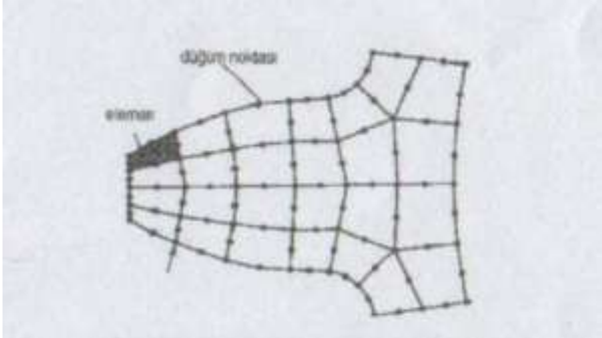

Figure 2: FEM Network and Element Structure **[27]**

In this study, the FEM analysis of the design was performed with ANSYS Maxwell program. The design, which is selected for material selection, winding arrangement and sizing with the ANSYS Maxwell RMxprt program, can then be magnetically analyzed using the Maxwell 2D program. The flow chart of the design made with the ANSYS Maxwell program is given in Figure (3).

Figure 3: FEM Analysis Flowchart with ANSYS Maxwell Program **[28]**

3. Results and Discussion

3.1 FEM Analysis Results

The designed $1500\ W, 1500\ rpm, 220\ V$, 9 Grooves and 8 Poles BLDC structure is given in Figure (4).

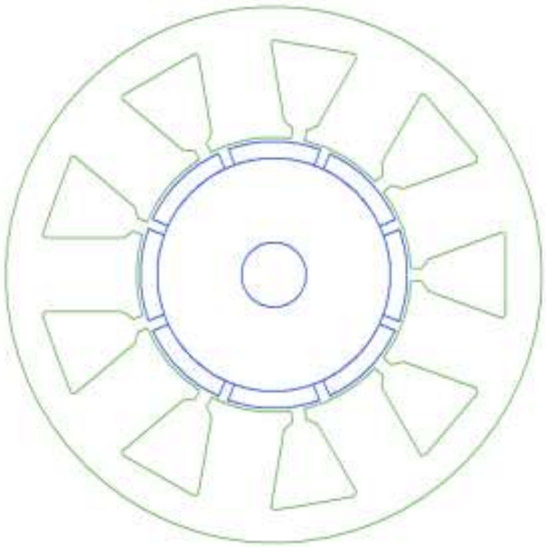

Figure 4:1500 W 1500 rpm Inner Rotor 9 Grooves 8 Poles Surface Magnet BLDC Appearance

When the results of the analysis were examined, it was seen that the values obtained from the FEM analysis and the values found by analytical calculation were similar.

Although the number of turns per phase was found to be $N = 118$ in the analytical calculations, when the FEM analysis was performed with this number of turns, the motor efficiency was found to be $\eta = 95.34\%$ and the rated speed was found to be $n = 1282$ rpm. For this reason, in order to increase the number of revolutions to the rated speed, the number of windings per phase in the design was optimized as $N = 102$ and the motor efficiency was calculated as $\eta = 96.24\%$ in this number of turns.

According to the FEM analysis results, BLDC input current and velocity change are given in Figure (5).

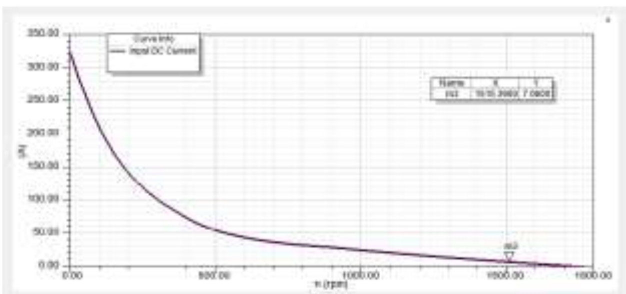

Figure 5: 1500 W 1500 rpm 220 V BLDC Input Current and Speed Change

When Figure (5) is examined, it is seen that the BLDC input current, which is found as $6.85\ A$ for $1500\ rpm$ velocity by analytical calculation, is compatible with the $7.06\ A$ current value for $1515\ rpm$ velocity calculated in ANSYS Maxwell FEM analysis.

According to the FEM analysis results, the BLDC Output Torque and Speed change are given in Figure (6). It is observed that the change of output torque over time varies in accordance with the BLDC characteristics.

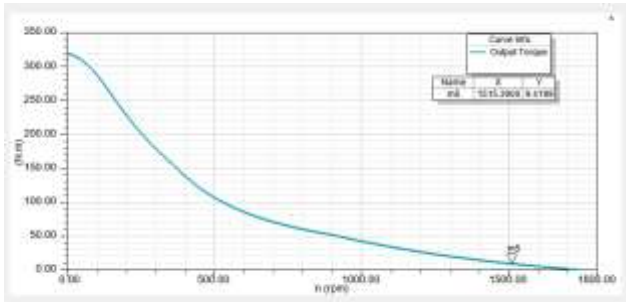

Figure 6:1500 W 1500 rpm 220 V BLDC Output Torque and Speed Change

According to the FEM analysis results, the change in BLDC Output Power and Speed is given in Figure (7). When Figure (7) is examined, it is seen that the BLDC, which is designed at the speed determined for the design, can provide the desired output power.

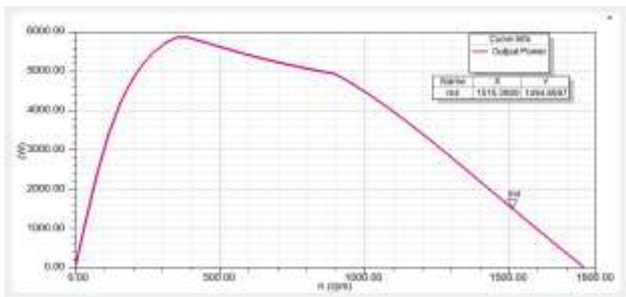

Figure 7: 1500 W 1500 rpm 220 V BLDC Output Power and Speed Change

According to the FEM analysis results, the change in BLDC Air Gap Flux Density is given by Figure (8). When Figure (8) is examined, it is understood that the air gap flux density distribution is uniform and suitable for the BLDC characteristic flux density distribution.

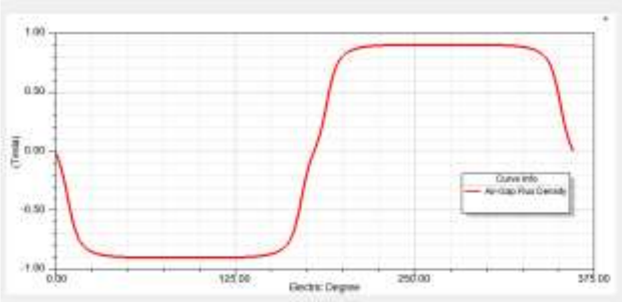

Figure 8: 1500 W 1500 rpm 220 V BLDC Air Gap Flux Density Change

According to the FEM analysis results, the BLDC Induced Phase and Line Voltage Shapes are given in Figure (9). It is observed that the line and phase voltage shapes of the design change smoothly and are suitable for the phase order and number.

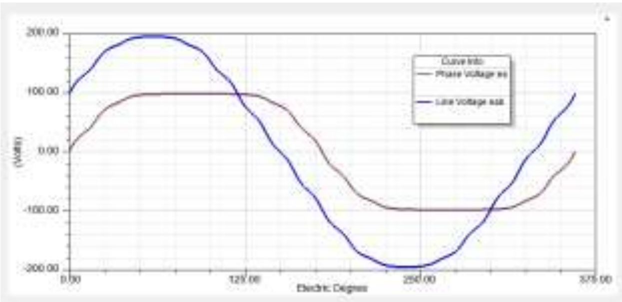

Figure 9: 1500 W 1500 rpm 220 V BLDC Induced Phase and Line Voltages at Rated Speed

According to the FEM analysis results, the change in BLDC Yield and Velocity is given in Figure (10). When the change of efficiency with speed is examined, it is noticed that the design is very close to the maximum efficiency at the specified speed. From this, it can be understood that the design is well optimized for the specified power and speed.

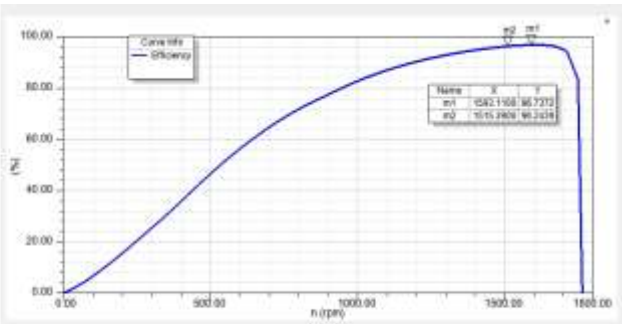

Figure 10: 1500 W 1500 rpm 220 V BLDC Yield and Speed Change

3.2. 2D Transient Analysis Results

After it was seen that the motor efficiency was at the desired level from the FEM analysis results performed with the ANSYS Maxwell program, 2D magnetic analysis was performed on the stator and rotor. In the magnetic analysis, it was observed that the magnetic flux distribution in the stator and rotor was uniform and there was no magnetic saturation in the material.

ANSYS Maxwell 2D Transient Analysis Vector Magnetic Flux Density View for $1500\, W, 1500\, rpm, 220\, V$, 9 Groove and 8 Pole BLDC design is given in Figure (11).

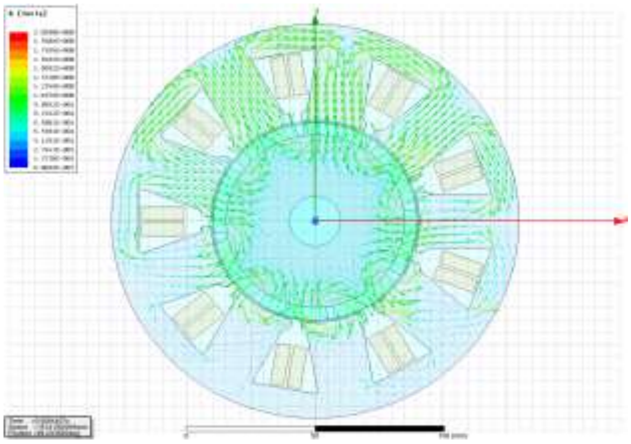

Figure 11: 1500 W 1500 rpm 220 V BLDC Vector Magnetic Flux Density View

ANSYS Maxwell 2D Transient Analysis Magnetic Flux Density View of $1500\, W, 1500\, rpm, 220\, V$, 9 Groove and 8 Pole BLDC design is given in Figure (12).

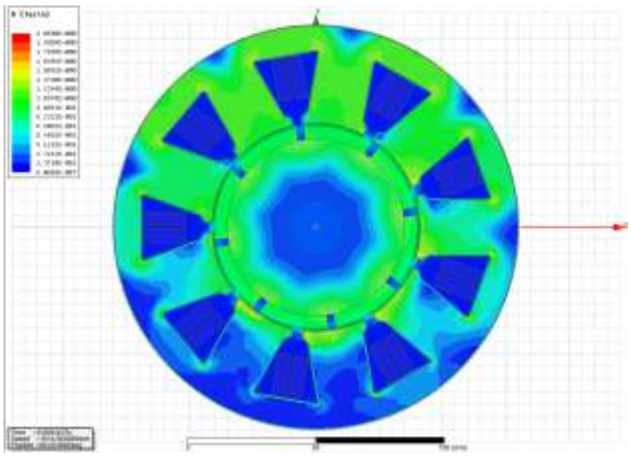

Figure 12:1500 W 1500 rpm 220 V BLDC Magnetic Flux Density View

ANSYS Maxwell 2D Transient Analysis Magnetic Field Strength for $1500\,W, 1500\,rpm, 220\,V$, 9 Groove and 8 Pole BLDC design is given in Figure (13).

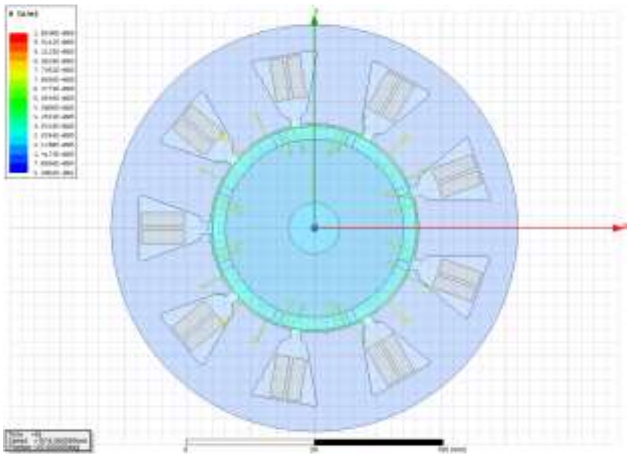

Figure 13: 1500 W 1500 rpm 220 V BLDC Vector Magnetic Field Strength View

The Ansys Maxwell 2D Transient Analysis Magnetic Field Intensity Distribution view of the designed $1500W, 1500\,rpm, 220\,V$ 9 $Groove\ and$ 8 $Pole$ BLDC is given in Figure (14).

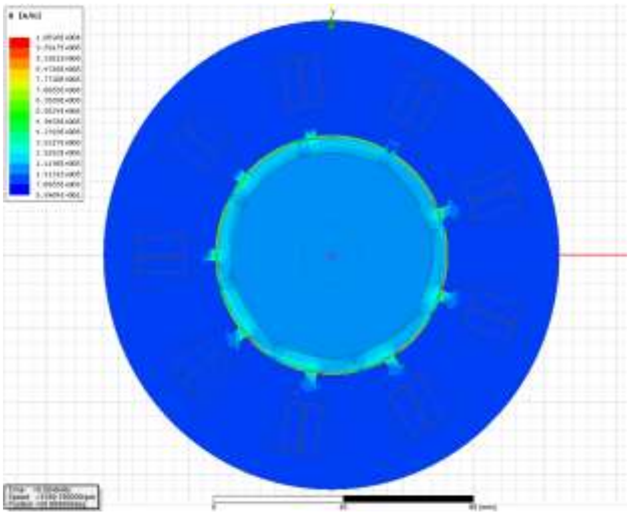

Figure 14: 1500 W 1500 rpm 220 V BLDC Manyetik Alan Şiddeti Dağılımı

The ANSYS Maxwell 2D Transient Analysis Cogging Moment Graph of $1500W$, $1500\,rpm$, $220\,V$, 9 $Groove\ and$ 8 $Pole$ BLDC is given in Figure (15)..

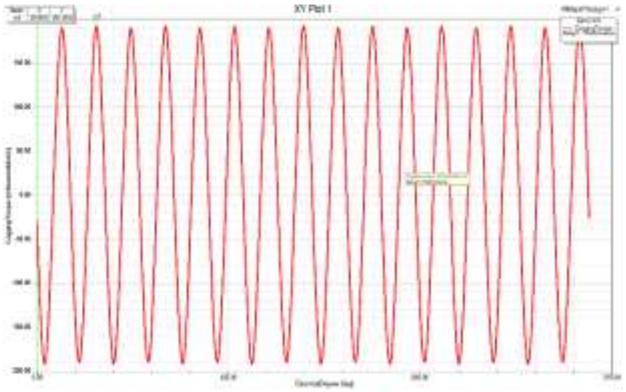

Figure 15:1500 W 1500 rpm 220 V BLDC Vuruntu Momenti Grafiği

The average stator tooth flux density of $1500W$, $1500\,rpm, 220\,V$ 9 $Groove$ and 8 pole BLDC was found to be $1.22T$ by FEM analysis performed with ANSYS Maxwell program and the Magnetic Flux Density Distribution in the Stator Teeth found by ANSYS Maxwell 2D Transient Analysis of the design is given in Figure (16).

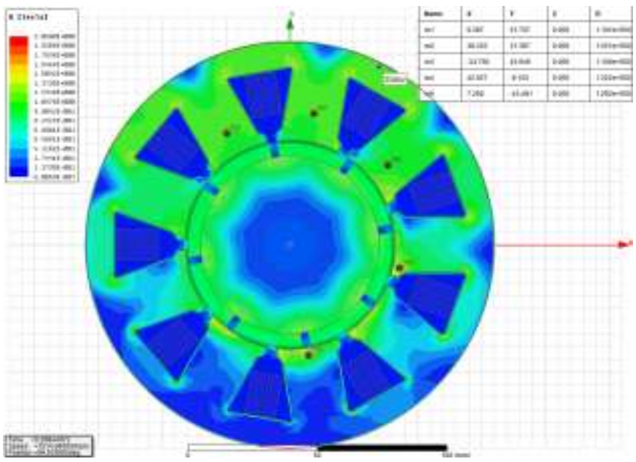

Figure 16:1500 W 1500 rpm 220 V BLDC Stator Dişlerindeki Manyetik Akı Yoğunluğu Dağılımı

When the results of the 2D magnetic analysis are examined, it is seen that the magnetic flux density is uniformly distributed on the BLDC geometry, with low cogging torque oscillation, there is no local saturation on the geometry and it is below the saturation limit for the steel material used.

3.3. Efficiency Class of Design

It is seen that the designed $1500\,W$, $1500\,rpm$, $220\,V$, 9 Groove and 8 Pole BLDC is in the IE4 class high efficiency motors class in IECC 60034-2-1-2014 Standards with η=95.34% efficiency.

4. Conclusion

In this study, an BLDC design of 1500 W, 1500 rpm, 220 V that can be supplied with single-phase mains voltage and used for general purposes was made. The analytical calculations required for sizing of the design were carried out with the MATLAB program, FEM analyzes and magnetic analyzes were carried out with the ANSYS Maxwell program. As a result of the simulation studies, it was seen that the design had maximum efficiency and efficiency in the number of rated revolutions. The design motor is in the IE4 class, which is the highest efficiency class according to IECC 60034-2-1-2014 Standards. The fact that the efficiency in the rated speed is very close to the maximum efficiency indicates that the design is well optimized for the rated values. The designed BLDC is suitable for general-purpose use and has high velocity and torque stability. In the magnetic analysis, it was observed that the magnetic flux density showed a uniform distribution on the designed motor geometry and there were no local saturation zones in the design. This indicates that the design will work efficiently and heating will not occur. The design can be used for general purposes without the need for additional cooling with single-phase mains voltage as intended.

Article Information

Financial Disclosure: The author (s) has not received any financial support for the research, authorship or publication of this study.

Authors' Contrtibution:

Halil Ercan Köksal: Concept, Design, Resources, Analysis, Literature Search, Writing Manuscript;

Muhammed Fatih ÇORAPSIZ: Concept, Supervision, Resources, Analysis, Literature Search, Critical Review.

Conflict of Interest/Common Interest: No conflict of interest or common interest has been declared by the authors.

Ethics Committee Approval: This study does not require ethics committee permission or any special permission.

References

[1] Brailsford, H.D,1955.Commutatorless Direct Current Motor. United States PatentOffice, https://patentimages.storage.googleapis.com/17/52/b4/893e9f63bed03f/US2719944.pdf. (2024).

[2] Wilson ,T. G. and Trickey,P. H.,1962.D-C machine with Solid-state Commutation. Electrical Engineering, 81(11), pp 879-884.

[3] Hendershot Jr, J.R. and Miller, TJE. , 1994. Design of Brushless Permanent – Magnet Motors. Magna Physics Publishing and Clarendon Press-Oxford, 566 p, Chelsea,Michigan.

[4] Yıldız,T., 2009. Fırçasız Doğru Akım Motorlarının Modellenmesi ve Kontrolü. Y.Lisans Tezi, Sakarya Üniversitesi Fen Bilimleri Enstitüsü,Sakarya.

[5] Rahideh,A.,Korakianitis,T.,Ruiz,P.,Keeble, T.,Rothman,M.T., 2010.Optimal Brushless Motor Design Using Genetic Algorithms. Journal of Magnetism and Magnetic Materials,322(22),pp 3680-3687.

[6] Güney, M.Z.,2024. Akıllı Soğutma Fan Uygulamaları İçin BLDC Motor Tasarımı.Y Lisans Tezi, Yıldız Teknik Üniversitesi Fen Bilimleri Enstitüsü,İstanbul.

[7] Kandemir, E., Duru, H.T., Çamur,S., Arifoğlu, B., Beşer,E.,2004. Fırçasız Doğru Akım Motor Sisteminin Deneysel Olarak Gerçekleştirilmesi ve Simülasyonu. ELECO'2004 Elektrik-Elektronik-Bilgisayar Mühendisliği Sempozyumu,Bursa.

[8] Ocak,C., 2013. Elektrikli Araçlar İçin Üç Kademeli Yeni Bir Fırçasız Doğru Akım Motoru Tasarımı Analizi ve Uygulaması.Doktora Tezi, Gazi Üniversitesi Fen Bilimleri Enstitüsü,Ankara.

[9] Aslan,N., 2020. Elekrikli Araçlar İçin Fırçasız Doğru Akım Motoru Tasarımı.Y.Lisans Tezi, Kahramanmaraş Sütçü İmam Üniversitesi Fen Bilimleri Enstitüsü, Kahramanmaraş.

[10] Virlan,B.,Munteaunu,A.,Livadaru,L.,Bobu, A.,Simion,A.,Nacu,I.,2021.Design and Optimization of a BLDC Motor for Small Power Vehicles.2021 International Conference on Electromechanical and Energy Systems,Lasi,Romania.

[11] Yetgin,A.G., 2020. Radyal Akı Yönlendirmeli Sabit Mıknatıslı Fırçasız DA Motorun Oluk-Kutup Sayısı Değişiminin Manyetik Akı Yoğunluğu Üzerindeki Etkisinin Belirlenmesi. Mehmet Akif Ersoy Üniversitesi Fen Bilimleri Enstitüsü Dergisi, 11(Ek Sayı 1), pp 256-265

[12] Hanselman, D., 2006. Brushless Permanent Magnet Motor Design Second Edition. Magna Pyhsics Publishing, 392 p, Ohio

[13] Hendershot Jr, J.R. and Miller, TJE. , 2010. Design of Brushless Permanent – Magnet Machines. Motor Design Books LLC,798 p, Chelsea,Michigan.

[14] Mergen, A.F. and Kocabaş, D.A., 2006. Elektrik Makineleri IV Doğru Akım Makineleri. Birsen Yayınevi,280 p, İstanbul.

[15] Çineli,B., 2024. Asimetrik Rotorlu Fırçası Doğru Akım Motoru Tasarımı. Y.Lisans Tezi, Kocaeli Üniversitesi Fen Bilimleri Enstitüsü,Kocaeli.

[16] Gürçay, M., 2024. Küçük Güçlü Daimi Mıknatıslı Bir Fırçasız Doğru Akim Motorunun Modellenmesi Ve Deneysel Sonuçlarının Çıkarılması.Y.Lisans Tezi, İstanbul Gedik Üniversitesi Lisansüstü Eğitim Enstitüsü, İstanbul.

[17] Nalakath,S.,Preindl,M.,Yang,Y.,Bilgin,B.,Cheng,B.,Emadi,A.,2015. Modelling and Analysis of Core Losses of an IPM Machine for Online Estimation Purposes.Yokohama, Japan

[18] Anonymous, 2018. Data sheet isovac 350-50 A. Austria, https://www.voestalpine.com/division_stahl/content/download/32782/347314/file/DB_isovac_350-50A_E_280715.pdf,&ved=2ahUKEwj17Kq8lbSNAxVqZ_EDHWyMBlcQFnoECBUQAQ&usg=AOvVaw2XNs4QXqF26vbSHxF-5V8i-(2025)

[19] Anonymous, 2022. Non grain oriented electrical steel powercore® Prodüktör range. Germany, https://www.thyssenkrupp-steel.com/media/content_1/publikationen/lieferprogramme/thyssenkrupp_product-range_no-electrical-steel_powercore_steel_en.pdf – (2025)

[20] Anonymous,2025.https://www.acroni.si/products/steel/category/flat-product/siwatt-m350-50a - (2025)

[21] Carunaiselvane,C.and Jeevananthan,S.,2012. Generalized procedure for BLDC motor design and substantiation in MagNet 7.1.1 software. 2012 International Conference on Computing, Electronics and Electrical Technologies [ICCEET], India.

[22] Mergen, A.F. and Kocabaş, D.A., 2007. Elektrik Makinalarında Sargılar. Birsen Yayınevi, 304 p, İstanbul.

[23] Ercan,A.A., 2014. Elektrik Motorlarının Verimlilik Standartları. Journal of ETA Maritime Science, Vol 2(1), pp 31-40.

[24] TSE Teknik Kurul, 2014. Döner elektrik makineleri - Bölüm 30-1: Şebeke tarafından beslenen a.a motorlar için verimlilik sınıfları (IE kodu). TSE, https://intweb.tse.org.tr/standard/standard/Standard.aspx?0811180511151080511041191101040550471051021200881110431131040730971190711170550490770511001040 43-(2025).

[25] Anonymous, 2018. https://library.e.abb.com/public/db64d153e3c346938e18916e66fb1d0d/9AKK107319%20EN%2005-2018_20848_ABB_Technical_note_IEC_60034_30_1.pdf - (2025).

[26] Güler, M.S, ve Şen, S., 2015. Sonlu Elemanlar Yöntemi Hakkında Genel Bilgiler. Ordu Üniversitesi Bilim ve Teknoloji Dergisi, 5(1), pp56-66

[27] Özdemir, A., 2006. Seramik Malzemelerin Kırılma Tokluğu Değerlerinin Üç Boyutlu Sonlu Elemanlar Yöntemi İle Teorik Olarak Belirlenmesi. Y.Lisans Tezi, Dokuz Eylül Üniversitesi Fen Bilimleri Enstitüsü, İzmir.

[28] Akar, M., Eker, M., Akın, F., 2021. BLDC Motor Design and Application for Light Electric Vehicle. Afyon Kocatepe Üniversitesi Fen ve Mühendislik Bilimleri Dergisi, 21()